



Published in final edited form as:

*Adv Funct Mater.* 2013 August 7; 23(29): 3628–3637. doi:10.1002/adfm.201203111.

## A Mechanistic Study of Wetting Superhydrophobic Porous 3D Meshes

**Stefan T. Yohe,**

Departments of Biomedical Engineering and Chemistry Boston University Boston, MA 02215, USA

**Jonathan D. Freedman,**

Departments of Biomedical Engineering and Chemistry Boston University Boston, MA 02215, USA

**Eric J. Falde,**

Departments of Biomedical Engineering and Chemistry Boston University Boston, MA 02215, USA

**Yolonda L. Colson,** and

Division of Thoracic Surgery Department of Surgery Brigham and Women's Hospital Boston, MA 02215, USA

**Mark W. Grinstaff\***

Departments of Biomedical Engineering and Chemistry Boston University Boston, MA 02215, USA

### Abstract

Superhydrophobic, porous, 3D materials composed of poly( $\epsilon$ -caprolactone) (PCL) and the hydrophobic polymer dopant poly(glycerol monostearate-*co*- $\epsilon$ -caprolactone) (PGC-C18) are fabricated using the electrospinning technique. These 3D materials are distinct from 2D superhydrophobic surfaces, with maintenance of air at the surface as well as within the bulk of the material. These superhydrophobic materials float in water, and when held underwater and pressed, an air bubble is released and will rise to the surface. By changing the PGC-C18 doping concentration in the meshes and/or the fiber size from the micro- to nanoscale, the long-term stability of the entrapped air layer is controlled. The rate of water infiltration into the meshes, and the resulting displacement of the entrapped air, is quantitatively measured using X-ray computed tomography. The properties of the meshes are further probed using surfactants and solvents of different surface tensions. Finally, the application of hydraulic pressure is used to quantify the breakthrough pressure to wet the meshes. The tools for fabrication and analysis of these superhydrophobic materials as well as the ability to control the robustness of the entrapped air layer are highly desirable for a number of existing and emerging applications.

## 1. Introduction

Superhydrophobic surfaces have large apparent contact angles which exceed  $150^\circ$  as a result of air maintained at the water-material interface.<sup>[1-9]</sup> The presence of air reduces the interfacial energy by minimizing the contact between water and the high surface area hydrophobic material. These surfaces are found in nature on animal fur, plant leaves, and insect legs, and are now commonly produced synthetically by adding surface roughness to a low surface energy material using a variety of processing techniques.<sup>[10-16]</sup>

The stability of the superhydrophobic surface state is key for many applications including corrosion prevention, reduction of biofouling, improving buoyancy, and self-cleaning.<sup>[17-26]</sup> In fact, some of these materials are able to maintain their superhydrophobic properties despite more stringent degassing conditions, including turbulent flow, surfactant addition, and increased water immersion depth.<sup>[27-35]</sup> These observations of stable surface superhydrophobicity are also supported by theoretical studies that have described such cases when an appropriate surface roughness, chemistry, and geometry are present.<sup>[36, 37]</sup>

We are interested in the fabrication and wetting of bulk 3D superhydrophobic materials. **Figure 1** demonstrates pictorially the difference between the wetting and superhydrophobic states in a 2D surface compared to a 3D structure. At a thin 2D surface, with a metastable superhydrophobic state, the loss of the entrapped air occurs relatively quickly with complete wetting of the surface. In contrast, a 3D structure maintains air at the surface and throughout the bulk material. Water infiltrates more slowly as a new water-air-material interface (i.e., superhydrophobic state) is continuously created as water penetrates into the material. One can envision how such a scenario would afford the use of superhydrophobic materials for applications distinct from those currently being considered for simple 2D superhydrophobic surfaces (e.g., drug delivery applications).

We recently reported the use of a superhydrophobic 3D mesh as a drug delivery device, and demonstrated the ability to control the stability of the bulk air layer which influences the rate of drug release. Use of a  $300\ \mu\text{m}$  thick superhydrophobic electrospun mesh enabled a sufficient concentration of drug to be loaded for an intended application and control of the wetting/air displacement to affect drug release.<sup>[38]</sup> Electrospinning was selected as the fabrication method for the mesh since there is significant precedence for this method in the literature.<sup>[14, 39-42]</sup>

Investigating the surface and bulk wetting properties of superhydrophobic meshes will be important for potential drug delivery applications<sup>[43-53]</sup> as well as for other industrial applications where time of wetting or loss of the superhydrophobic property is crucial to function. Consequently, characterizing and understanding the superhydrophobic state in a mesh and identifying the advantages and limitations of these materials are critical. Herein, we report the: 1) relationships between mesh fiber size, surface fill fraction, and surface chemistry on hydrophobicity; 2) rate of water infiltration into electrospun meshes with varying hydrophobicity using quantitative 3D X-ray imaging; 3) dependence of contact angle on changes in surface tension or with surface adsorption events; 4) critical surface

tension of a solvent required to infiltrate into an electrospun mesh; and 5) applied hydraulic pressure required for initial water breakthrough through the meshes.

## 2. Results and Discussion

In order to characterize the stability of the superhydrophobic state in electrospun meshes we performed a number of material and physio-chemical experiments to: 1) determine the contact angle of the meshes as a function of polymer composition, mesh formulation, and fiber size; 2) measure the rate of water penetration into the mesh; 3) assess the role of surface energy on the phenomena; and 4) identify the requisite pressure to transition from the Cassie to the Wenzel state of wetting.

### 2.1. Chemistry and Fabrication of the Meshes

The superhydrophobic 3D materials under investigation are electrospun poly( $\epsilon$ -caprolactone) (PCL) and poly(glycerol monostearate-co- $\epsilon$ -caprolactone) (PGC-C18), where PCL is doped with PGC-C18 in different proportions to tailor the overall superhydrophobic state. PGC is a copolymer of caproic acid and glycerol (4:1), where the glycerol subunit can be modified with various pendant groups to impart functionality or alter the hydrophilicity/hydrophobicity of the polymer.<sup>[54, 55]</sup> In this study, stearic acid was added to produce a hydrophobic polymer (PGC-C18) to slow, or prevent, water penetration into the mesh. The presence of a large number of hydrophobic stearate ( $-\text{O}(\text{O})\text{C}(\text{CH}_2)_{16}\text{CH}_3$ ) pendant groups leads to a decrease in the surface energy of the doped meshes. Undoped PCL electrospun meshes are modestly hydrophobic with an apparent contact angle of  $123^\circ$ . Adding PGC-C18 to PCL increases the apparent contact angle of the electrospun meshes to  $150^\circ$  with 30 wt% PGCC18 doping (20 wt/v% electrospinning solution) (**Figure 2**). The stearate modification is required for the superhydrophobic effect, since electrospun PCL with doped PGC-OH, which lacks the stearate group, has no apparent contact angle ( $\text{ACA} = 0^\circ$ ) and wets with the application of a water droplet. The molecular weight of PGC-C18 is much lower than the PCL used in these studies (20 kDa vs. 70-90 kDa). Therefore, increasing the amount of PGC-C18 also leads to a decrease in electrospinning solution viscosity and subsequent decrease in fiber size.<sup>[56, 57]</sup> With 10% PGC-C18 doping there is a modest decrease in fiber size compared to PCL ( $7.7 \mu\text{m}$  vs.  $7.2 \mu\text{m}$ ), and a greater decrease with 30% PGC-C18 doping ( $2.46 \mu\text{m}$ ). Thin ( $50 \mu\text{m}$ ) and thick ( $500 \mu\text{m}$ ) electrospun meshes of these compositions possessed the same apparent contact angle, which supports the concept that as water penetrates into the mesh it will see a new superhydrophobic water-air-material interface.

### 2.2. Polymer Hydrophobicity, Mesh Fiber Size, Surface Roughness, and Contact Angle Measurements

Changes in polymer hydrophobicity and electrospun fiber size contribute to superhydrophobicity, as both the surface energy and the proportion of air exposed at the surface (i.e., air fill fraction) influence the overall superhydrophobic state.<sup>[41, 58, 59]</sup> In order to observe changes in polymer surface energy, we compared the contact angles of flat PCL-PGC-C18 blended surfaces to the electrospun meshes. Solvent cast films prepared from PCL, PCL with 10% PGC-C18, and PCL with 30% PGC-C18 have contact angles of

83°, 109°, and 111°, respectively, where an increase in the hydrophobic polymer dopant PGC-C18 to PCL leads to a larger contact angle, and thus a lower surface energy. All of the contact angles for the cast films are lower than the contact angle values for the corresponding meshes (121°, 143°, 150°, respectively), confirming the presence of entrapped air at the surface of the mesh and the property of superhydrophobicity for those PCL meshes doped with 30% PGC-C18. Next, the fiber size of the electrospun meshes was altered to study the effect of surface roughness and surface fill fraction on superhydrophobicity by modifying the electrospinning solution and processing parameters. **Figure 3** shows the resultant apparent contact angle for the three superhydrophobic mesh chemistries as a function of changes in fiber size/surface roughness. All meshes have porosities of 80-90%; micrometer-sized fiber meshes had lower porosities, and decreasing fiber size led to an increase in porosity. PCL electrospun meshes were produced with fiber sizes ranging from 166 nm to 7.7  $\mu\text{m}$ . The smallest fibers lead to an apparent contact angle of 141°, whereas the largest fiber had an apparent contact angle of 123°. This result was expected, as it is known that decreasing the surface fill fraction of a surface, or reducing the amount of polymer exposed at a given surface (and increasing the air fraction), will result in a higher apparent contact angle. The 10% PGC-C18 and 30% PGC-C18 doped PCL meshes initially follow this trend (where a decrease in fiber size leads to an increase in apparent contact angle), but exhibit an eventual decrease in contact angle with continued fiber size reduction. Specifically, the 10% PGC-C18 doped PCL meshes reached a maximum apparent contact angle of 148° with a fiber size of 2.7  $\mu\text{m}$ , followed by a decrease to 142° with 123 nm fibers. The 30% PGCC18 meshes reached a maximum apparent contact angle of 157° with 641 nm fibers, and the apparent contact angle decreased to 149.3° for the 296 nm fibers. One possible explanation for this increase and subsequent decrease in apparent contact angle with fiber size reduction is that the PGC-C18 is partitioning to the surface of the fibers. Polymers of different compositions are known to phase separate, both within the bulk and at the surface of the material.<sup>[60, 61]</sup> Differential scanning calorimetry experiments indicate that phase separation within the bulk of the electrospun meshes does not occur, as PCL and PGC-C18 are sufficiently chemically similar.<sup>[38]</sup> However, phase separation at the surface may be occurring to reduce the surface energy at an interface, which is commonly observed with polymer blends both on flat and textured material surfaces.<sup>[60-65]</sup> Our results suggest that the hydrophobic soft chain stearate segment of our copolymer preferentially partitions to the material surface such that a significant hydrophobic effect is observed with modest additions of PGC-C18. With large fibers, the exposed surface becomes easily saturated with these highly hydrophobic pendant groups. However, as the surface area to volume ratio becomes larger, as a consequence of a decrease in fiber size, the same PGCC18 content is insufficient to cover the fiber surface and generate the same hydrophobic effect. With 10% PGC-C18 doping, superhydrophobicity begins to decrease with fiber sizes below 2.8  $\mu\text{m}$ , with the underlying PCL bulk material contributing to the surface composition. Increasing the doping to 30% PGCC18 in PCL meshes provides three times the amount of stearate groups to functionalize this larger surface area, but there is still an eventual decrease in the apparent contact angle at a smaller fiber size. Usually a decrease in surface fill fraction from smaller fibers leads to a higher apparent contact angle, as is seen in single phase PCL meshes. However, the addition of PGC-C18 presents a competing mechanism, where higher concentrations of PGC-C18 are required to cover the

increased surface area produced with small fibers to maintain the superhydrophobic effect. PCL meshes with 50% PGC-C18 doping were fabricated next to confirm these competing effects. The largest fibers produced (8.7  $\mu\text{m}$ ) have an apparent contact angle of  $142^\circ$ , while the smallest fibers (206 nm) have an apparent contact angle of  $169^\circ$ , demonstrating that superhydrophobicity continues to increase with a reduction in fiber size, and that 50% PGC-C18 is sufficient to functionalize a larger surface area.

### 2.3. Regeneration of the Superhydrophobic State After Wetting

Next, we determined whether the superhydrophobic state of a mesh could be revitalized after repetitive wetting. Three superhydrophobic meshes from the previous study (PCL with 30% PGC-C18, ACA =  $157^\circ$ ) were wetted, where the meshes were first dipped in ethanol for 5 s to remove the air layer, and subsequently immersed into a water bath for 12 h. The meshes were then removed from water and dried at ambient conditions for 5 h. The contact angle of the superhydrophobic mesh was then measured. This procedure was repeated two more times for a total of three cycles. After three cycles of wetting and drying, the contact angle of the meshes was not significantly different ( $<3^\circ$ ), demonstrating that the surface does not become permanently wetted after exposure to water, and that superhydrophobic property is reversible and returns after the water is removed.

### 2.4. Mesh Superhydrophobicity and Performance Studies

The short and long-term stability of the air layer in superhydrophobic electrospun meshes is important for a given application. The presence or absence of air within the meshes was confirmed by the observation that meshes float with air present (and sink when not), air bubbles can be released from meshes after applying a sufficient pressure (i.e., squeezing them) to them while underwater, and using clinical ultrasound to visualize the wet and dry states.<sup>[66]</sup> In order to characterize the stability of the Cassie state (non-wetting state) of these superhydrophobic mesh formulations, we measured the wetting and water infiltration rate of a series of superhydrophobic 3D meshes. Specifically, we further characterized the PCL (7.7  $\mu\text{m}$ ,  $123^\circ$ ), 10% PGC-C18 doped PCL (7.2  $\mu\text{m}$ ,  $142^\circ$ ), 30% PGCC18 doped PCL (2.4  $\mu\text{m}$ ,  $150^\circ$ ), and 50% PGC-C18 doped PCL (169 nm,  $168^\circ$ ) meshes using a number of physio-chemical techniques (Figure 3). These mesh formulations were selected to span a range of superhydrophobicities, fiber sizes, and surface chemistries. The current interpretation for the large apparent contact angle with these meshes is that the entrapped air layer in PCL meshes is weakly metastable, but the addition of PGC-C18 to PCL affords a more robust air layer at the surface and throughout the bulk material.

### 2.5. Water Infiltration Measurements

A number of researchers have assessed long-term underwater stability of superhydrophobic surfaces using techniques such as the reflection of light,<sup>[28,67]</sup> oxygen sensing<sup>[33]</sup>, and fluid dynamics.<sup>[29–31,68]</sup> Since we are interested in determining the stability of the air throughout these bulk superhydrophobic materials, we chose instead to use quantitative X-ray microcomputed tomography ( $\mu\text{CT}$ ) to measure the rate and depth of water infiltration. A 3:1 water-ioxaglate solution (an anionic iodinated CT contrast agent) was incubated with the superhydrophobic electrospun meshes and the depth/rate at which water penetrated into the mesh was determined from the CT signal as the contrast agent solution wetted the mesh.

**Figure 4** shows the results of this study pictorially, where the progression of water infiltration is tracked through the cross section of a representative mesh for PCL, PCL with 10% PGC-C18, and PCL with 30% PGC-C18. The infiltration rate into super-hydrophobic meshes is plotted in **Figure 5**, where PCL is fully wetted within ten days and all air has been displaced within the meshes. Approximately 80% of the air is displaced within two days, followed by the removal of the remaining 20% of air in the following eight days. The weakly metastable state of entrapped air within PCL allows for eventual removal of all air. The more hydrophobic electrospun PCL meshes with 10% PGC-C18 doping are also metastable, but show a much slower, sustained displacement of air, where an average of 52% of air has been displaced by 77 days. Finally, PCL with 30% PGC-C18 showed a stable air layer over the length of the study, with only 1% of air displaced over 35 days and water is only observed at the outer superhydrophobic material surface. A follow up scan of 30% PGC-C18 doped PCL electrospun meshes after 75 days of incubation showed <4% of the meshes had been infiltrated, demonstrating prolonged underwater stability of the Cassie state. A linear regression analysis of the water infiltration data revealed that PCL, PCL with 10% PGC-C18, and PCL with 30% PGC-C18 showed infiltration rates of 13.5, 2, and 0.07  $\mu\text{m}/\text{day}/\text{side}$ , respectively, which corresponds to 5.4%, 0.8%, and 0.03% total infiltration (both sides) per day for 500  $\mu\text{m}$  meshes. Differences in infiltration rates were statistically significant using an analysis of covariance (ANCOVA) ( $p < 0.01$ ). The PCL mesh with 50% PGC-C18 doping was not studied since water infiltration would be even slower as it is more hydrophobic than the 30% PGC-C18 containing meshes. The results of this study support the conclusions that both PCL and PCL with 10% PGCC18 doping are in the metastable state where water infiltrates the mesh and displaces entrapped air, and that 30% PGC-C18 doping leads to a stable Cassie state where the air layer is permanently maintained.

## 2.6. Surfactant Studies

The Cassie state of wetting that defines superhydrophobicity is a result of an interaction between a low surface energy material and a high surface tension liquid (i.e., PCL-PGC-C18 meshes and water). Air is maintained at the material-liquid surface reducing formation of a high energy interface. The superhydrophobic characteristics of a surface are decreased or removed with changes in the surface energy of either phase, either with an increase in the surface energy of the material surface or a decrease in the surface tension of the liquid. The use of surfactants is one method to modulate the energy of either/both phase(s),<sup>[69–71]</sup> where surfactants decrease the surface tension (ST) of water by lowering the energy of the air-water interface, or alternatively, the hydrophobic domains of the surfactant can bind the hydrophobic material surface to increase the energy of the surface. The effect that a particular surfactant has on water surface tension and material surface energy will depend on both the surfactant structure as well as the extent of adsorption.

We used two common surfactants, sodium dodecyl sulfate (SDS) and polysorbate 20, to determine the dependence of the superhydrophobic state on exposure to surfactants. The charged SDS surfactant was used at two different concentrations (0.001 M, 0.01 M), where the SDS was added to the probing solution for apparent contact angle measurements (**Figure 6**). By adding SDS to the probing medium, we assessed the effect of a decrease in water surface tension since insufficient time was provided for SDS to adsorb to the mesh

surface.<sup>[70]</sup> The difference ( ) in apparent contact angle between water and SDS containing solutions was statistically significant when comparing any pair of mesh chemistries (i.e., PCL vs. PCL with 10% PGC-C18 with 0.001 M SDS;  $p$ -value < 0.001). Application of droplets containing 0.001 M (ST  $\approx$  63 mN/m)<sup>[72]</sup> to electrospun PCL meshes resulted in no apparent contact angle (i.e., complete wetting), compared to 123° for water alone. Application of 0.001 M SDS solutions to electrospun PCL meshes with 10%, 30%, and 50% PGC-C18 resulted in lower apparent contact angles compared to water, where increased PGC-C18 showed less of a reduction in contact angle ( 47°, 13°, and 6° respectively). A ten-fold increase in the SDS concentration (0.01 M; ST  $\approx$  35 mN/m) provided a sufficient drop in surface tension to fully wet the 10% and 30% PGC-C18 doped PCL meshes. The 50% PGC-C18 containing meshes were not completely wetted, though a significant drop in the apparent contact angle to 109° ( 60° from water) was observed.

The effect of the neutral polysorbate 20 surfactant on mesh superhydrophobicity was examined under two conditions: 1) surfactant was added to the water probe in a manner similar to the above SDS experiments and 2) by soaking electrospun meshes in polysorbate 20 solutions prior to exposure to a water droplet. These experiments enabled us to study how a decrease in surface tension alters the superhydrophobic characteristics of the meshes using a second surfactant, as well as to examine how long term incubation allows adsorption of surfactant to a mesh surface, leading to an increase in surface energy. The effect of polysorbate 20 concentration on apparent contact angle when added to the water probe was performed at three concentrations (0.001 M, 0.01 M, 0.1 M). Surface tension values for all of solutions are  $\approx$ 40 mN/m, and all concentrations are above the critical aggregation concentration for polysorbate 20.<sup>[73]</sup> The difference in apparent contact angle between the surface and water or surface and a polysorbate 20 containing solution was statistically significant when comparing any pair of mesh chemistries (i.e., PCL vs. PCL with 10% PGC-C18 with 0.1 M polysorbate 20;  $p$ -value < 0.01), except between 30% PGC-C18 and 50% PGC-C18 meshes with 0.001 M solutions, and 10% PGC-C18 and 30% PGC-C18 meshes with 0.01 M solutions. When probing PCL mesh surfaces, all concentration of polysorbate 20 probing solutions led to immediate penetration of the solution, and no apparent contact angle was observed (**Figure 7A**). Adding 10%, 30%, and 50% PGC-C18 to PCL electrospun meshes stabilized the entrapped air layer, and only showed a modest decrease in apparent contact angle for all polysorbate 20 concentrations, where even the largest polysorbate 20 concentration (0.1 M) was not sufficient to wet the meshes ( 19°, 11°, 3°, respectively, for 0.1 M solutions). We then incubated superhydrophobic meshes in polysorbate 20 solutions (0.0001–0.1 M) for 24 h, after which samples were air-dried and probed using pure water. In this procedure, the polysorbate 20 had adsorbed to the surface of the meshes. The resulting polysorbate 20 treated meshes possessed a significantly reduced apparent contact angle (**Figure 7B**). PCL electrospun meshes wetted with water after exposure to all polysorbate 20 concentrations. Adding 10% PGC-C18 to the PCL mesh affords a slightly more robust entrapped air layer, with an apparent contact angle observed for only the lowest polysorbate 20 concentration used for incubation ( 10° for 0.0001 M solution). The surfaces were incrementally more robust with addition of 30% PGC-C18, and an apparent contact angle was detected for the two lowest concentrations selected ( 1° for 0.001 M; 10° for 0.0001 M). PCL meshes with 50% PGC-C18 formed an apparent contact angle with all but the

highest polysorbate 20 solution (0.1 M), with apparent contact angle changes of 0°, 14°, 40° for solutions with 0.0001 M, 0.001 M, and 0.01M polysorbate 20. The difference in apparent contact angle between meshes with and without polysorbate 20 incubation was statistically significant when comparing any pair of superhydrophobic mesh chemistries (i.e., PCL vs. PCL with 50% PGC-C18 with 0.01 M polysorbate 20; p-value < 0.01), except between 30% PGC-C18 and 50% PGC-C18 meshes with 0.001 M polysorbate 20 incubation.

## 2.7. Critical Surface Tension Measurements

We next expanded on our surfactant studies by creating a “modified Zisman curve” for each of the superhydrophobic mesh chemistries. Zisman curves are used to probe flat surfaces, where solvents of different surface tensions are used to identify the critical surface tension in which there is no observable contact angle. We adapted this method to characterize the meshes and used solvents possessing different surface tension values to probe the mesh surface, ranging from water (72 mN/m) to ethanol (22 mN/m). In this experiment, the critical surface tension corresponds to an apparent contact angle of 0°, or one where there is no barrier to immediately absorb into the electrospun material.

PCL electrospun meshes were determined to have a critical surface tension of 57 mN/m, where only a small decrease from the surface tension of water (72 mN/m) resulted in no barrier for wetting (**Figure 8**). The entrapped air layer was more robust for PGC-C18 doped meshes as compared to PCL alone. PCL with 10% PGC-C18 formed an apparent contact angle with solvents with surface tensions as low as 44 mN/m, and PCL with 30% PGC-C18 formed an apparent contact angle until 39 mN/m. PCL with 50% PGC-C18 formed an apparent contact angle with solvents with surface tensions as low as 33 mN/m. Solvents exposed to these materials below these surface tension values resulted in complete wetting, where, for example, ethanol treatment results in complete wetting for all mesh types. A best-fit line was then calculated, which approximated the surface tension required for a 50% reduction in apparent contact angle from pure water for each superhydrophobic mesh chemistry. These values were found to be 60.6, 40, 34.7, 30 mN/m for PCL, PCL with 10% PGC-C18, PCL with 30% PGC-C18, and PCL with 50% PGC-C18, respectively, which closely match critical surface tension values that lead to complete infiltration (57, 39, 33, 27.6 mN/m). The small difference in surface tension for a 50% reduction in apparent contact angle and complete infiltration shows that the stability of the superhydrophobic state drops quickly as the critical surface tension is approached. Critical surface tension values for complete wetting found in this study are also consistent with our surfactant studies, where PCL meshes wetted below surface tensions of 63 mN/m, 10% and 30% PGC-C18 were shown to wet below 35 mN/m, and 50% PGC-C18 meshes did not wet in contact with solutions with surface tensions of 35 mN/m.

## 2.8. Water Breakthrough Measurements

We also studied the pressures required for water to infiltrate into the superhydrophobic meshes using a filtration setup. This water pressure value typically signifies the transition from a Cassie state (air entrapped) to a Wenzel state (air removed) for superhydrophobic materials.<sup>[74,75]</sup> Water pressure applied to the electrospun meshes was increased to the point of initial wetting and breakthrough observed. PCL electrospun meshes were easily wetted,



with only 2.5 kPa of water pressure necessary to induce this transition (**Figure 9**). Increasing the PGC-C18 doping in PCL meshes raised the barrier to wetting with a 2.9-fold increase (7.3 kPa) in the pressure required to cause breakthrough with the 10% PGC-C18 doped meshes. A 4.5-fold increase (11.3 kPa) in the pressure was required for breakthrough over PCL meshes for 30% PGC-C18 doped PCL. The difference in breakthrough pressure between any pair of meshes was statistically significant ( $p$ -value < 0.001). In general, decreased porosity increases breakthrough pressure. However, the PGC-C18 containing PCL meshes have higher breakthrough pressures even though they possess slightly greater porosities (and thus greater total air content) signifying that superhydrophobicity plays a major role. Meshes with 50% PGC-C18 doping could not be evaluated, as the meshes tore before infiltration of water occurred.

### 3. Conclusion

In summary, superhydrophobic 3D meshes were fabricated from PCL with varying amounts of PGC-C18 using the electrospinning technique. We directly measured the infiltration of water into the electrospun meshes using X-ray computed tomography, enabling us to characterize the stability of the entrapped air layer within PCL meshes doped with various amounts of the hydrophobic polymer dopant PGC-C18. Next, we identified the boundary conditions at which this superhydrophobicity can function, and when the effect can be removed. The addition of surfactant to the water droplet led to a decrease in entrapped air stability within superhydrophobic meshes through a decrease in water surface tension, and likewise adsorption of a surfactant to the mesh surface also increases the surface energy of the mesh. Solvents of varying surface tensions were then used to estimate the critical surface tension and wetting of the mesh. Finally, hydraulic pressure was applied to the meshes to find the requisite pressure to cause water breakthrough and transition from the Cassie state of wetting to the Wenzel state. Overall, the results from these fundamental studies provide a means to: 1) fabricate polymeric superhydrophobic meshes using the electrospinning method; 2) establish guidelines to design a specific mesh property; and 3) employ techniques and procedures to characterize these types of superhydrophobic compositions. Continued investigation of superhydrophobic materials will lead to new knowledge and their evaluation in a number of biomedical and industrial applications.

### 4. Experimental Section

*Materials:* All solvents were purchased from Sigma (St. Louis MO) without further purification. Stannous 2-ethylhexanoate,  $\epsilon$ -caprolactone, stearic acid,  $N,N'$ -dicyclohexylcarbodiimide, and 4-(dimethylamino) pyridine were purchased from Sigma. Palladium on carbon was purchased from Strem Chemicals. Poly( $\epsilon$ -caprolactone) (70,000-90,000 MW) was purchased from Sigma. 5-benzyloxy-1,3-dioxan-2-one was prepared as previously reported.<sup>[54]</sup> All reactions were performed under nitrogen atmosphere unless otherwise noted. NMR spectra were recorded on a Varian INOVA spectrometer (1H at 400 MHz). Chemical shifts were referenced to residual solvent peaks ( $\text{CHCl}_3$  peak at 7.24 ppm). DCM = dichloromethane, THF = tetrahydrofuran, DCC =  $N,N'$ -dicyclohexylcarbodiimide, DCU = dicyclohexylurea, DMAP = 4-(dimethylamino) pyridine,

PCL = poly( $\epsilon$ -caprolactone), PGC-C18 = poly(glycerol monostearate-co- $\epsilon$ -caprolactone), Pd/C = 10% palladium on activated carbon, and PBS = phosphate buffered solution.

*Synthesis of Poly(glycerol Monostearate-co- $\epsilon$ -caprolactone) (PGCC18):* Poly(glycerol monostearate-co- $\epsilon$ -caprolactone), or PGC-C18, was prepared as previously reported.<sup>[54]</sup> Briefly,  $\epsilon$ -caprolactone and 5-benzyloxy-1,3-dioxan-2-one monomers were mixed at a 4:1 molar ratio in a schlenk flask and subsequently evacuated and flushed with N<sub>2</sub> three times. Sn(Oct)<sub>2</sub> was used (M/I = 500) to catalyze the ring-opening polymerization of the co-monomers at 140°C for 18 h, and the resulting copolymer was isolated by precipitation in cold methanol (99% yield). The benzyl-protecting groups on the copolymer were removed via palladium-catalyzed hydrogenation overnight in THF, and filtered through Celite (95% yield). The deprotected polymer, stearic acid, DCC, and DMAP were dissolved in DCM and stirred at room temperature for 18 h. Precipitated DCU was filtered and the solvent evaporated. The product, PGC-C18, was dissolved in DCM and precipitated in cold methanol. The polymer was filtered and dried by evaporation (93% yield).

*Size Exclusion Chromatography (SEC):* Molecular weight determinations were performed via size exclusion chromatography using THF as the eluent on a Polymer Laboratories PLgel 3  $\mu$ m MIXED-E column (3  $\mu$ m bead size) and a Rainin HPLC system (temp = 25°C; flow rate = 1.0 mL/min). Polystyrene standards (Polysciences, Inc.) were used for calibration. PGC-C18 was shown to have a Mn = 21,100 and a polydispersity of Mw/Mn = 1.73.

*Formation of Doped and Undoped Poly( $\epsilon$ -caprolactone) Meshes:* All electrospinning solutions were 5-40 w/v% and prepared in a solvent mixture of 5:1 chloroform/methanol. Undoped PCL electrospinning solutions were prepared by dissolving PCL in chloroform and allowing full dissolution. This was followed by adding methanol with rigorous vortexing. Doped PCL electrospinning solutions were prepared in a similar fashion, where 10, 30, or 50 wt% of PCL was replaced with PGC-C18. Solutions were loaded into a glass syringe and placed into a syringe pump set at a flow rate of 10 mL/h. A 12–18 kV high voltage lead was applied at the base of the syringe needle. A grounded rotating collector was covered in aluminum foil and placed 9–24 cm away from the needle. Meshes were fabricated with a total thickness of 300  $\mu$ m, except for those meshes used for the water infiltration experiment, which had a thickness of 500  $\mu$ m. Porosity measurements of the meshes were determined by measuring the mass and volume with a known material density. Exact pore sizes of electrospun meshes are ill-defined as the meshes are composed of a random array of fibers, and one can only calculate a surface pore size. Mathematical models are best used to describe average pore size of meshes, and further information on doing so can be found in the provided references.<sup>[76,77]</sup>

*Fiber Morphology and Characterization:* Samples for scanning electron microscopy (SEM) were prepared by mounting meshes on an aluminum sample stub and then sputter-coated with a 5 nm layer of gold-palladium alloy. Samples were then imaged on a Zeiss SUPRA 40VP field emission scanning electron microscope using an accelerating voltage of 2 kV. Fiber size was analyzed using Image J, where all fibers in a representative SEM image were sized to characterize the mesh.

*Apparent Contact Angle Measurements:* Hydrophobicity and surface energy of electrospun meshes were assessed by apparent contact angle measurements using microdrop analysis (Kruss DSA100 Goniometer) with deionized water at 20°C. Microdrop analysis was selected over other prominent techniques for measuring contact angles on rough material surfaces due to relative ease in the experimental setup and sufficient accuracy for the studies.<sup>[9,10,16,78–84]</sup> The first study involved the application of a 3 µL droplet of water, water with polysorbate 20 (0.001-0.1 M) (CAC =  $1.7 \times 10^{-5}$  M)<sup>[73]</sup>, or water with SDS (0.001-0.01 M) (CAC = 0.008 M)<sup>[72]</sup> to the surface for measurement, and fit using Young-Laplace mode. Contact angle measurements were taken 30 s after droplet placement to minimize time for surfactant to adsorb and to avoid evaporation. In the second study, the electrospun meshes were soaked in polysorbate 20 solutions (0.0001-0.1 M) for 24 h to allow for surface adsorption, after which the meshes were removed and air dried for 24 h. Contact angles of meshes incubated in the latter way were probed with water alone to determine the effect of surfactant adsorption to the surface. Statistical significance between apparent contact angle measurements of superhydrophobic meshes was performed using a Student's t-test.

*Measuring Contrast Agent Infiltration Using µCT:* Electrospun meshes were incubated in an 80 mgI/mL aqueous solution of Ioxaglate (Hexabrix; an anionic iodinated CT contrast agent) for 28–77 days, and were periodically scanned using a µCT imaging system at an isotropic voxel resolution of 18 µm<sup>3</sup>, 70 kVP tube voltage, 114 µA current, and 300 ms integration time. Surface tension of the water-Hexabrix solution was 72 mN/m (measured by pendant drop at 20°C). The sequential slices obtained using the µCT system were then converted into the standard image format (DICOM) using the proprietary software from Scanco Medical. This data was then analyzed using commercial image processing software (Analyze, BIR, Mayo Clinic, Rochester, MN, USA). The 3D µCT data sets were imported into Analyze where a representative cross-section of each electrospun mesh type (PCL, PCL with 10% PGCC18, and PCL with 30% PGC-C18) was analyzed at multiple timepoints over the duration of the study to compare relative infiltration. The total distance that water had penetrated into each electrospun mesh type ( $n = 3$ ) was then quantitatively measured using a volumetric measurement (100 pixels × 100 pixels) through the thickness of the mesh, where pixel values >1500 were considered to be infiltrated, and pixel values <1500 were not considered to be infiltrated. This volumetric measurement resulted in a fraction or% of water infiltration, where an infiltration depth/rate could then be calculated with a known mesh thickness (500 µm). A linear regression was fit to infiltration data in order to calculate the infiltration rate of each electrospun mesh type. Statistical significance between infiltration rates of 3D superhydrophobic meshes was analyzed using analysis of covariance (ANCOVA) with Prism 5.0d (GraphPad, La Jolla, CA) ( $F = 8.8$ ,  $DOF = 2,12$ ,  $p = 0.0044$ ).

*Modified Zisman Curve:* A modified Zisman curve was constructed for the four electrospun mesh types used in this study. An apparent contact angle of 0°, or no apparent contact angle, was defined as the critical surface tension (ST) of the meshes. Meshes were probed with a series of different solvents that span a large range of surface tensions (highest to lowest): water (72 mN/m), glycerol (64 mN/m), dimethyl sulfoxide (44 mN/m), benzyl alcohol (39 mN/m), 1,4-dioxane (33 mN/m), 1-octanol (28 mN/m), acetone (25 mN/m), and ethanol (22

mN/m). Surface tension values are at solvent-air interface at 20°C, and were obtained from the chemical vendor. Ethanol-water solutions were prepared to probe PCL meshes to better resolve a critical surface tension for infiltration. PCL meshes were wetted with an application of a 10% ethanol solution (57 mN/m).<sup>[85]</sup> A double exponential curve was used to fit the apparent contact angle data (curve fitting toolbox, Matlab, Matlab 2011a, Natick, MA). The best fit curves were used to approximate the surface tension required to produce a 50% drop in apparent contact angle relative to the apparent contact angle formed with water.

*Superhydrophobic Mesh Burst Pressure:* Electrospun meshes were tested to determine the critical pressure (“burst pressure”) to switch from a Cassie state of wetting to a Wenzel state of wetting. A modified water level was used, where electrospun meshes were attached to one side of the level in order to allow water pressure to be applied. The side of the water level attached to the electrospun mesh infiltration setup was lowered at 1 cm per 5 s to increase the applied water pressure. The burst pressure was recorded as the applied water pressure where the mesh was first wetted. Increasing beyond the burst pressure allowed water to freely flow through the electrospun mesh. The 50% PGC-C18 fractured before water infiltration, thus, preventing determination of a burst pressure value. Statistical significance between superhydrophobic mesh burst pressures was performed using a Student's t-test. Tap water was used for these studies.

## Acknowledgments

This work was supported in part by BU Training Grant in Pharmacology and Experimental Therapeutics, BU MSE Innovation Grant, BU Nanotheranostics ARCBWH, Boston University's Nanomedicine Program and Cross-Disciplinary Training in Nanotechnology for Cancer NIH R25 CA153955, and NIH R01CA149561.

## References

1. Ma M, Hill RM. *Curr. Opin. Colloid Interface Sci.* 2006; 11:193.
2. Roach P, Shirtcliffe NJ, Newton MI. *Soft Matter.* 2008; 4:224.
3. Nakajima A, Hashimoto K, Watanabe T. *Monatsh. Chem.* 2001; 132:31.
4. Rothstein JP. *Annu. Rev. Fluid Mech.* 2010; 42:89.
5. Lafuma A, Quere D. *Nat. Mater.* 2003; 2:457. [PubMed: 12819775]
6. Patankar NA. *Langmuir.* 2004; 20:7097. [PubMed: 15301493]
7. Wang S, Jiang L. *Adv. Mater.* 2007; 19:3423.
8. Gao L, McCarthy TJ. *J. Am. Chem. Soc.* 2006; 128:9052. [PubMed: 16834376]
9. Acatay K, Simsek E, Ow-Yang C, Menciloglu YZ. *Angew. Chem. Int. Ed.* 2004; 43:5210.
10. Li X-M, Reinhoudt D, Crego-Calama M. *Chem. Soc. Rev.* 2007; 36:1350. [PubMed: 17619692]
11. Xue CH, Jia ST, Zhang J, Ma JZ. *Sci. Technol. Adv. Mater.* 2010; 11:033002.
12. Yan Y, Gao N, Barthlott W. *Adv. Colloid Interface.* 2011; 169:80.
13. Feng X, Jiang L. *Adv. Mater.* 2006; 18:3063.
14. Ma M, Hill RM, Rutledge GC. *J. Adhes. Sci. Technol.* 2008; 22:1799.
15. Levkin PA, Svec F, Fréchet JMJ. *Adv. Funct. Mater.* 2009; 19:1993. [PubMed: 20160978]
16. Tuteja A, Choi W, Ma M, Mabry JM, Mazzella SA, Rutledge GC, McKinley GH, Cohen RE. *Science.* 2007; 318:1618. [PubMed: 18063796]
17. Nosonovsky M, Bhushan B. *Curr. Opin. Colloid Interface Sci.* 2009; 14:270.
18. Zhang X, Shi F, Niu J, Jiang Y, Wang Z. *J. Mater. Chem.* 2008; 18:621.
19. Genzer J, Efimenko K. *Biofouling.* 2006; 22:339. [PubMed: 17110357]
20. Marmur A. *Biofouling.* 2006; 22:107. [PubMed: 16581675]

21. Yao X, Song Y, Jiang L. *Adv. Mater.* 2011; 23:719. [PubMed: 21287632]
22. Voronov RS, Papavassiliou DV, Lee LL. *Ind. Eng. Chem. Res.* 2008; 47:2455.
23. Plawsky JL, Ojha M, Chatterjee A, Wayner Jr PC. *Chem. Eng. Commun.* 2008; 196:658.
24. Verplanck N, Coffi nier Y, Thomy V, Boukherroub R. *Nanoscale Res. Lett.* 2007; 2:577.
25. Heikenfeld J, Dhindsa M. *J. Adhes. Sci. Technol.* 2008; 3:319.
26. Gao L, McCarthy TJ. *Langmuir.* 2007; 23:9125. [PubMed: 17661500]
27. Bobji MS, Kumar SV, Asthana A, Govardhan RN. *Langmuir.* 2009; 25:12120. [PubMed: 19821621]
28. Poetes R, Holtzmann K, Franze K, Steiner U. *Phys. Rev. Lett.* 2010; 105:166104. [PubMed: 21230986]
29. McHale G, Newton MI, Shirtcliffe NJ. *Soft Matter.* 2010; 6:714.
30. Ou J, Rothstein JP. *Phys. Fluids.* 2005; 17:103606.
31. Truesdell R, Mammoli A, Vorobieff P, Van Swol F, Brinker CJ. *Phys. Rev. Lett.* 2006; 97:044504. [PubMed: 16907578]
32. Gao X, Jiang L. *Nature.* 2004; 432:36. [PubMed: 15525973]
33. Shirtcliffe NJ, McHale G, Newton MI, Perry CC, Pyatt FB. *Appl. Phys. Lett.* 2006; 89:104106.
34. Liu T, Yin Y, Chen S, Chang X, Cheng S. *Electrochim. Acta.* 2007; 52:3709.
35. Zhang H, Lamb R, Lewis J. *Sci. Technol. Adv. Mater.* 2005; 6:236.
36. Marmur A. *Langmuir.* 2006; 22:1400. [PubMed: 16460052]
37. Fukagata K, Kasagi N, Koumoutsakos P. *Phys. Fluids.* 2006; 18:089901.
38. Yohe ST, Colson YL, Grinstaff MW. *J. Am. Chem. Soc.* 2012; 134:2016. [PubMed: 22279966]
39. Acatay K, Simsek E, Ow-Yang C, Menciloglu YZ. *Angew. Chem. Int. Ed.* 2004; 43:5210.
40. Ma M, Gupta M, Li Z, Zhai L, Gleason KK, Cohen RE, Rubner MF, Rutledge GC. *Adv. Mater.* 2007; 19:255.
41. Ma M, Mao Y, Gupta M, Gleason KK, Rutledge GC. *Macromolecules.* 2005; 38:9742.
42. Papadopoulou S, Tsiptsias C, Pavlou A, Kaderides K, Sotiriou S, Panayiotou C. *Colloid Surf. A.* 2011; 387:71.
43. Wu P, Grainger DW. *Biomaterials.* 2006; 27:2450. [PubMed: 16337266]
44. Langer R, Tirrell DA. *Nature.* 2004; 428:487. [PubMed: 15057821]
45. Kopecek J, Yang JY. *Polym. Int.* 2007; 56:1078.
46. Hoare TR, Kohane DS. *Polymer.* 2008; 49:1993.
47. Wolinsky JB, Colson YL, Grinstaff MW. *J. Controlled Release.* 2012; 159:14.
48. Kim S, Kim J-H, Jeon O, Kwon IC, Park K. *Eur. J. Pharm. Biop-harm.* 2009; 71:420.
49. Langer R. *Chem. Eng. Commun.* 1980; 6:1.
50. Weinberg BD, Blanco E, Gao J. *J. Pharm. Sci.* 2007; 97:1681. [PubMed: 17847077]
51. Hoffman AS. *J. Controlled Release.* 2008; 132:153.
52. Exner AA, Saidel GM. *Expert Opin. Drug Delivery.* 2008; 5:775.
53. De Souza R, Zahedi P, Allen CJ, Piquette-Miller M. *Drug Delivery.* 2010; 17:365. [PubMed: 20429844]
54. Wolinsky JB, Ray III WC, Colson YL, Grinstaff MW. *Macromolecules.* 2007; 40:7065.
55. Wolinsky JB, Yohe ST, Colson YL, Grinstaff MW. *Biomacro-molecules.* 2012; 13:406.
56. Doshi J, Reneker DH. *J. Electrostat.* 1995; 35:151.
57. Deitzel JM, Kleinmeyer J, Harris D, Beck Tan NC. *Polymer.* 2000; 42:261.
58. Cortese B, D'Amone S, Manca M, Viola I, Cingolani R, Gigli G. *Langmuir.* 2008; 24:2712. [PubMed: 18217778]
59. Gao L, McCarthy TJ. *Langmuir.* 2006; 22:2966. [PubMed: 16548542]
60. Yoon SC, Ratner BD. *Macromolecules.* 1986; 19:1068.
61. Thomas HR, O'Malley JJ. *Macromolecules.* 1979; 12:323.
62. Xu X, Zhuang X, Chen X, Wang X, Yang L, Jing X. *Macromol. Rapid Commun.* 2006; 27:1637.
63. Xu X, Yang L, Wang X, Chen X, Liang Q, Zeng J, Jing X. *J. Controlled Release.* 2005; 108:33.

64. Yang Y, Li X, Qi M, Zhou S, Weng J. Eur. J. Pharm. Biopharm. 2008; 69:106. [PubMed: 18078743]
65. Desnoyer, J.; Hossainy, S.; Pacetti, S.; Tang, Y. 2005. WO Patent 2,005,121,264
66. Yohe ST, Herrera VLM, Colson YL, Grinstaff MW. J. Controlled Release. 2012; 162:92.
67. Fadeeva E, Truong VK, Stiesch M, Chichkov BN, Crawford RJ, Wang J, Ivanova EP. Langmuir. 2011;27. [PubMed: 22142229]
68. Lee C, Kim CJ. Phys. Rev. Lett. 2011; 106:14502.
69. Mohammadi R, Wassink J, Amirfazli A. Langmuir. 2004; 20:9657. [PubMed: 15491199]
70. Ferrari M, Ravera F, Rao S, Liggieri L. Appl. Phys. Lett. 2006; 89:053104.
71. Chang F-M, Sheng Y-J, Chen H, Tsao H-K. Appl. Phys. Lett. 2007; 91:094108.
72. Mysels KJ. Langmuir. 1986; 2:423.
73. Nino MRR, Patino JMR, Am J. Oil Chem. Soc. 1998; 75:1241.
74. Cassie ABD, Baxter S. Trans. Faraday Soc. 1944; 40:546.
75. Wenzel RN. J. Ind. Eng. Chem. 1936; 28:988.
76. Pan N. Tex. Res. J. 1993; 63:336.
77. Rawal A. Langmuir. 2012; 28:3285. [PubMed: 22251513]
78. Wagner H. J. Appl. Phys. 1990; 67:1352.
79. Yamaki JI, Katayama Y. J. Appl. Polym. Sci. 1975; 19:2897.
80. Carroll B. J. Colloid Interface Sci. 1976; 57:488.
81. Berim GO, Ruckenstein E. J. Colloid Interface Sci. 2005; 286:681. [PubMed: 15897087]
82. Zhu M, Zuo W, Yu H, Yang W, Chen Y. J. Mater. Sci. 2006; 41:3793.
83. Kang M, Jung R, Kim HS, Jin HJ. Colloid Surf. A. 2008; 313:411.
84. Agarwal S, Horst S, Bognitzki M. Macromol. Mater. Eng. 2006; 291:592.
85. Vazquez G, Alvarez E, Navaza JM. J. Chem. Eng. Data. 1995; 40:611.

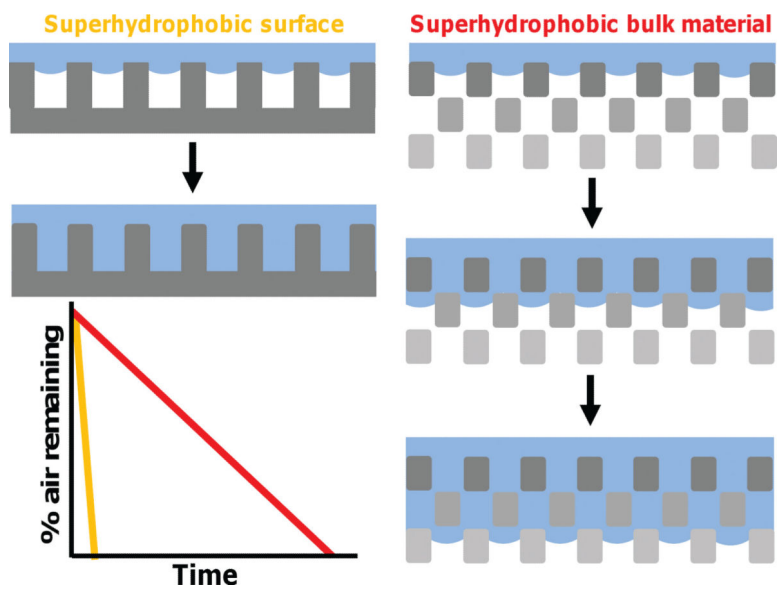


**Figure 1.** Comparison between the behavior of a 2D superhydrophobic surface (left) and a superhydrophobic 3D material (right). A 2D super-hydrophobic surface, when metastable, will lose all of the air entrapped at the interface relatively quickly and become wetted. In comparison, a metastable superhydrophobic bulk 3D material will loss air over time as water infiltrates more slowly as a new water-air-material interface (i.e., superhydrophobic state) is continuously created.

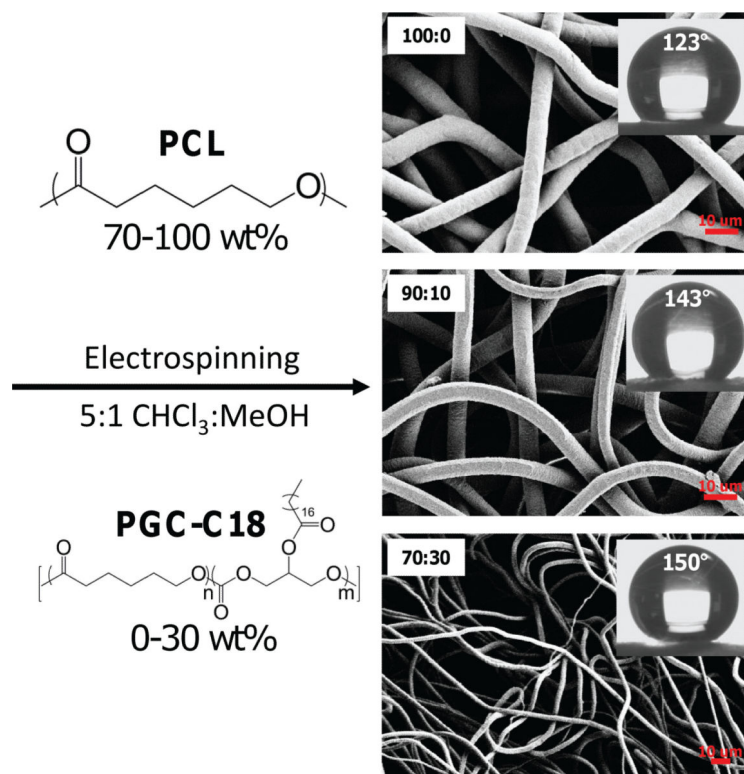


**Figure 2.** Superhydrophobic 3D materials were produced by electrospinning. By varying the amount of the hydrophobic polymer dopant PGCC18, the apparent contact angle was increased by virtue of a lower surface energy and higher surface roughness. Meshes shown in the microscopy images were spun with 20 wt/v% polymer electrospinning solutions.



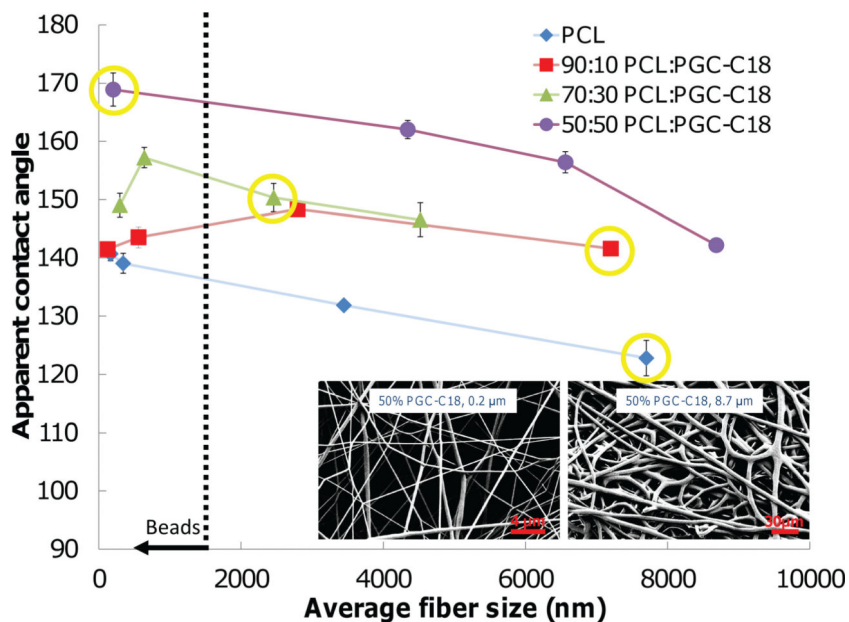


**Figure 3.** Apparent contact angle dependence on electrospun fiber size for four superhydrophobic mesh chemistries. PCL and PCL with 50% PGC-C18 meshes show a continued increase in apparent contact angle with a decrease in fiber size. 10% and 30% PGC-C18 meshes have an initial increase in apparent contact angle, followed by a decrease. Inset shows 50% PGC-C18 micro- and nanofibers, where fiber size is modified through changes in the electrospinning parameters selected. Fibers with diameters below 1500 nm showed a beads-on-a-string morphology. Formulations highlighted in yellow were selected for further study to span a range of superhydrophobicity. ( $N = 3$ ; average  $\pm$  SD)

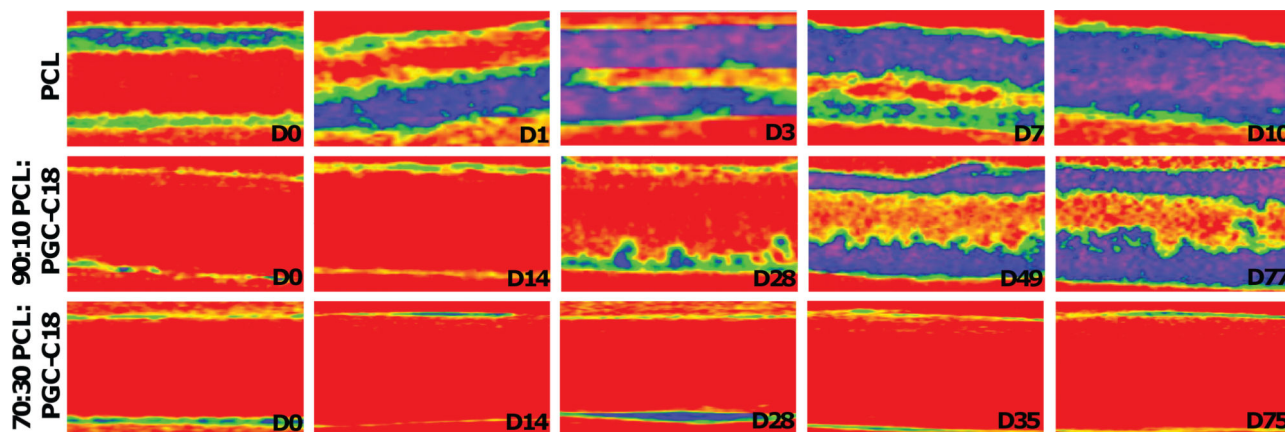


**Figure 4.** Cross-sectional images of the kinetic infiltration of water into PCL, PCL with 10% PGC-C18, and PCL with 30% PGC-C18 from Day 0 (D0) to as long as 77 days (D77). Water quickly infiltrates into PCL electrospun meshes (unwetted meshes shown in red with increasing water content progressing from yellow to green to blue). Adding 10% PGC-C18 affords a metastable superhydrophobic state, where water slowly infiltrates over time. Adding 30% PGC-C18 achieves a stable superhydrophobic state and water only penetrates the surface of the material. Meshes were 500  $\mu\text{m}$  thick.

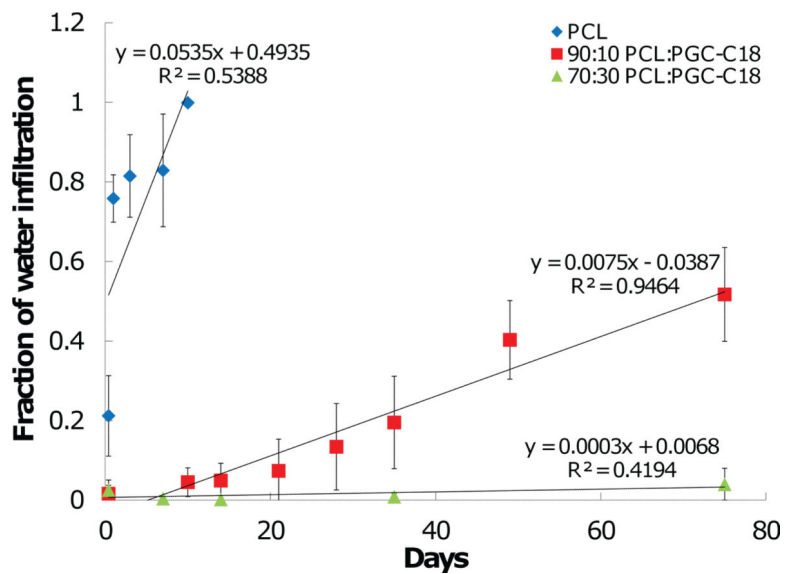


**Figure 5.** Degree of water infiltration within superhydrophobic electro-spun meshes over time. Increasing PGC-C18 and superhydrophobicity leads to slower removal of entrapped air and thus slower wetting. ( $N = 3$ ; average  $\pm$  SD).

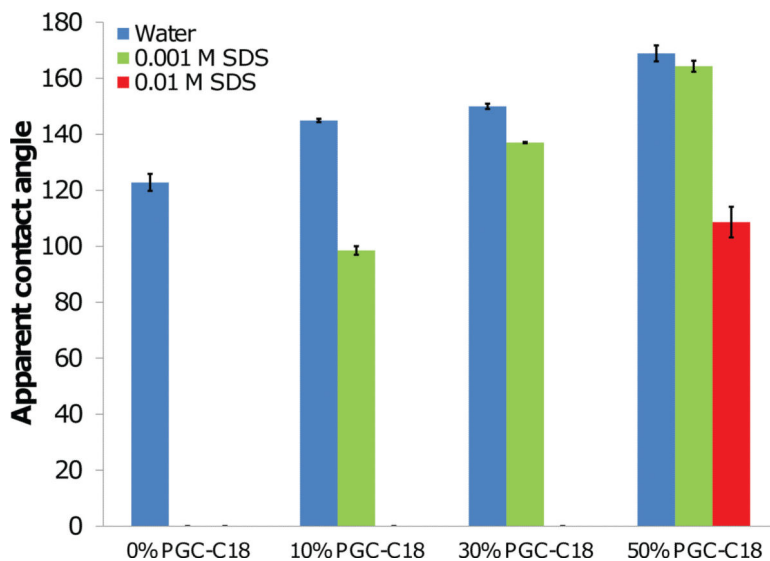


**Figure 6.** Apparent contact angle measurements for superhydrophobic electrospun meshes when probed with water or water containing SDS. With 0.001 M SDS, PCL meshes did not form an apparent contact angle, and meshes containing 10%, 30%, or 50% PGC-C18 had lower apparent contact angles compared to water alone. Increasing the SDS concentration by 10-fold in the probing solution resulted in no apparent contact angle for all superhydrophobic mesh chemistries other than 50% PGC-C18, where instead a significant drop in apparent contact angle is observed. ( $N = 3$ ; average  $\pm$  SD).

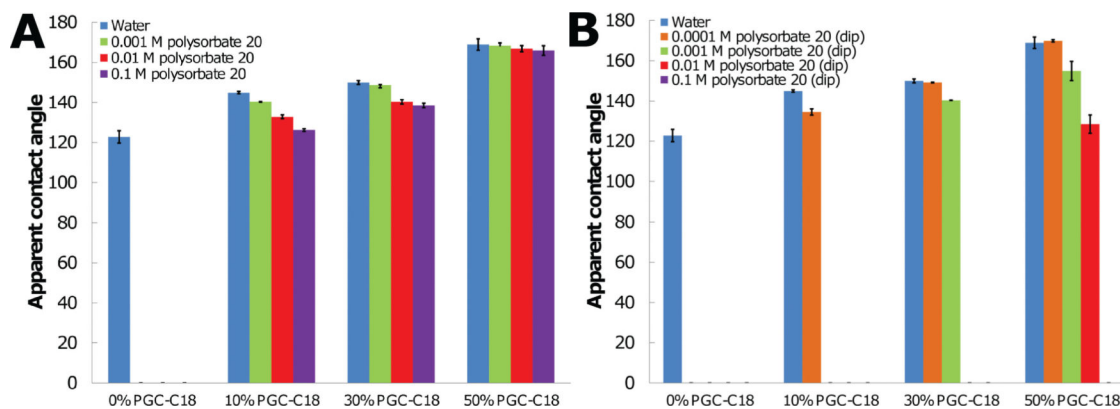


**Figure 7.**

Apparent contact angles of superhydrophobic electrospun meshes when A) probed with polysorbate 20 solutions or B) after 24-h incubation in polysorbate 20 solutions and probed with water. PCL electrospun meshes are completely wetted with polysorbate 20 solution probes and after mesh incubation for all concentrations. In contrast, PCL with 10%, 30%, and 50% PGC-C18 doping only showed a modest decrease in contact angle with polysorbate 20 probes. Incubating 10% and 30% PGC-C18 doped meshes with polysorbate 20 solutions allowed wetting to occur much more readily, with apparent contact angles only observed at the lowest polysorbate 20 concentrations. 50% PGC-C18 meshes are only wetted when incubated with the highest concentration of polysorbate 20. ( $N = 3$ ; average  $\pm$  SD).

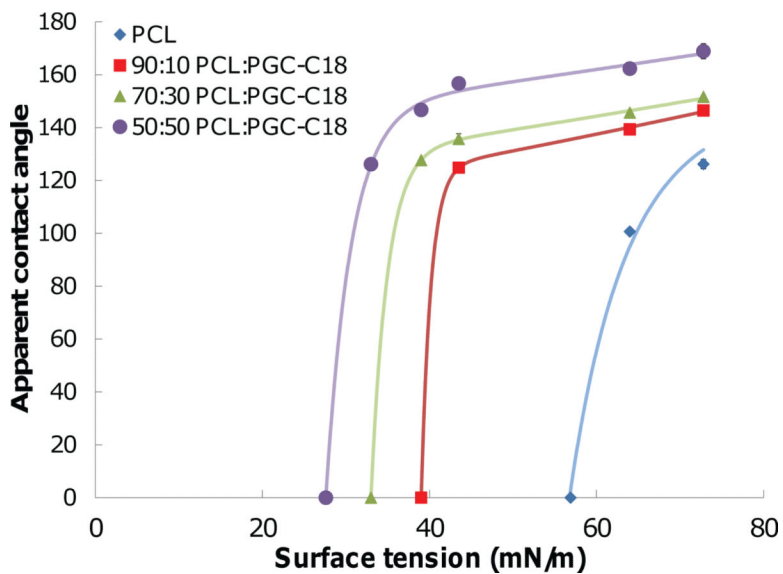


**Figure 8.** Measurement of apparent contact angles using solvents with varied surface tension to determine the critical surface tension required for immediate infiltration into superhydrophobic electrospun meshes. PCL meshes are easily wetted, while increasing PGC-C18 content and superhydrophobicity affords a more robust entrapped air layer in the porous meshes to prevent solvent infiltration. Best fit curves were double exponential. ( $N = 3$ ; average  $\pm$  SD).

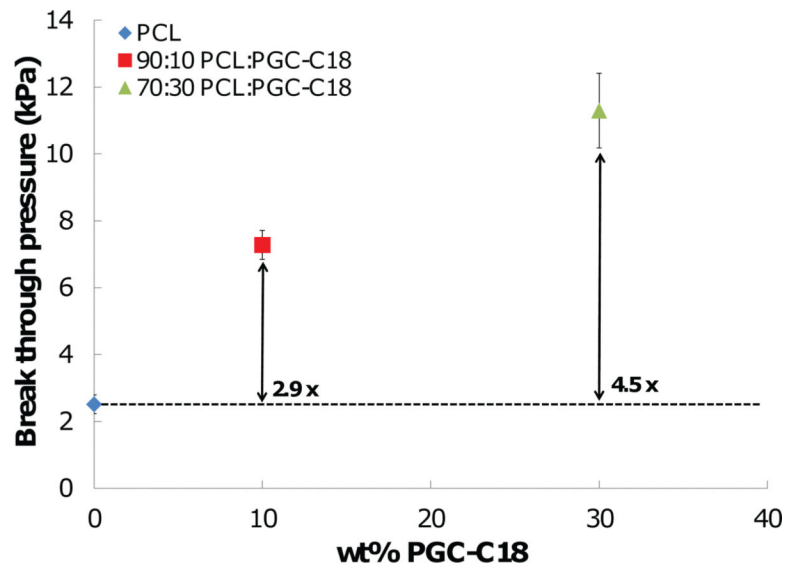


**Figure 9.** Break through pressures required to force water from the Cassie state to the Wenzel state of wetting. Increasing the PGC-C18 content increases the amount of pressure necessary to cause water to breakthrough. Meshes using 50% PGC-C18 fractured before infiltration, and could not be used in this study. ( $N = 3$ ; average  $\pm$  SD).